Dual-Targeting OH2 Oncolytic Virus Therapy Overcomes Immune Resistance in TNBC via PD-L1/DDR1 Silencing and GM-CSF Expression

Shuoyu Hu[1a], Jiaqi Liu[2b], Zongwen Xu[3,c *], Haojia Xue[4d]

[1]Homeschool, Guizhou, 550002, China
[2]Nanjing Foreign Language School, Nanjing, 210018, China
[3]Nakornpayap International School, Chiangmai, 50300, Thailand
[4]Experimental High School Attached to Beijing Normal University, Beijing, 100000, China

Abstract: Triple-negative breast cancer (TNBC) is an aggressive subtype of breast cancer, accounting for between 15% and 20% of cases and remains resistant to conventional treatments due to the absence of active receptors, high metastatic potential and a strongly immunosuppressive tumour microenvironment. Here, we propose the oncolytic herpes simplex virus type 2 (OH2), which was rationally designed as a dual-purpose therapeutic platform, Recombinant OH2 was designed to express a small forked RNA (shRNA) that silences both the discoid domain receptor (DDR1) and programmed death ligand 1 (PD-L1) , while incorporating the surviving promoter to limit viral replication in cancer cells and thus reduce off-target cytotoxicity. In addition, OH2 encodes granulocyte-macrophage colony-stimulating factor (GM-CSF) to enhance dendritic cell activation and immune cell capture . Simultaneous silencing of DDR1 and PD-L1 alters extracellular matrix remodelling and weakens tumour immune evasion. In addition, OH2-mediated suppression of β-catenin signalling indirectly relieves T cell blockade, collectively stimulating the infiltration of $CD8^+$ T lymphocytes and natural killer cells into the tumour microenvironment. In vitro, therapeutic efficacy is evaluated using human and murine TNBC cell lines (e.g., MDA-MB-231, 4T1) with Western blotting, qPCR, ELISA and luciferase assays. In vivo, we use xenograft models in humanised NSG mice, which have been reconstituted with CD34+ haematopoietic stem cells , as well as genetically modified Myc;Ptenfl/fl mice, which develop spontaneous breast tumours. Translational challenges — including potential immune clearance of the viral vector, tumour heterogeneity, and intratumoral delivery constraints — are considered in the experimental design and discussed as directions for future refinement. This strategy combines tumour-specific oncolytic action, modulation of immune checkpoints, and matrix reprogramming to increase tumour immunogenicity and overcome the resistance mechanisms characteristic of TNBC. Our results indicate that this dual-purpose OH2 construct represents a promising new-generation oncolytic viral therapy. Together, these findings establish OH2 as a multifunctional immuno-oncolytic platform with strong potential for clinical translation in refractory TNBC.

1. Introduction

Triple negative breast cancer (TNBC) represents about 15-20% of the breast cancer cases, and it is the most aggressive and treatment-resistant subtypes [1]. Due to lack of estrogen receptor (ER), progesterone receptor (PR), and HER2 amplification [2]. TNBC is characterized by a suppressive tumor micro environment (TME) which limits T cell infiltration and enhances immune evasion, making common immune checkpoint blockade (ICB) ineffective [3], [4]. TNBC incorporates 2 major mechanisms that drive immune suppression: PD-L1 Signaling pathway and DDR1-mediated extracellular matrix (ECM) remodeling [5]. PD-L1, expressed on tumor and stromal cells, binds to PD-1 on T and NK cells, leading to immune exhaustion and tolerance [6]. DDR1, a collagen receptor tyrosine kinase, organizes the ECM into dense, aligned structures that physically restrict tumor-infiltrating lymphocytes (TILs) [7], [8].

The following explains the 3 foundational papers that we used as the base of our research. The first study combined 2 chemoimmunotherapy regimens in TNBC- paclitaxel (PTX) with atezolizumab (ATZ),

[a]shuoyuhueducation@gmail.com, [b]liuremy25@gmail.com
[c]kevin.xvzw@gmail.com, [d]jennyxue225@gmail.com

each referred to as PD-L1 blockade. Nab-paclitaxel and atezolizumab promote the expansion of T memory stem (Tsem) and T follicular helper (Tfh) cells while preventing T cell dysfunction and exhaustion. Mast cells—typically associated with allergic reactions—were also found to play a role in tumor biology. Their activation enhances the efficacy of PD-L1 blockade.enhancing mast cell activation or infiltration could potentially improve anti-tumor immunity in TNBC [9].

In the second study, it was found that DDR1 helps organize collagen into thick, tightly packed fibers, which act like a wall, keeping T cells out. But when they removed DDR1 from the cancer cells in mice with working immune systems, the tumors shrank — because the T cells were finally able to enter the tumor and execute their effector functions. Interestingly they found that it was the extracellular domain (ECD) of DDR1 that was enough to realign collagen and keep T cells out. Therefore, developing anti-DDR1 therapies could help to enhance therapeutic efficacy [10].

In tumor, beta-catenin and WNT pathways are usually overly activated, which will lead to metastasis and self-renewal of tumor cells, and inhibit the infiltration of T cells. In the third study, it was found that the UL41 protein in oncolytic herpes simplex virus type 2 (OH2) can suppress the expression of the beta-catenin effector molecule and downregulate the downstream gene matrix metalloproteinase (MMP). Also, OH2 has reduced off-target activity, which reduces the overall toxicity of treatment [11].

Though the three foundational papers offer innovative insights into the treatment of triple-negative breast cancer (TNBC), their therapeutic efficacy remains limited. While these treatments enhance T-cell infiltration and promote immune cell activation, they may also result in robust immune activation leading to inflammation. Furthermore, since DDR1 is expressed in normal tissues, its inhibition could lead to physiological disruptions. Therefore, minimizing off-target effects is critically important. The therapeutic strategy proposed in this study is specifically targeted toward tumors and simultaneously employs three distinct inhibitors and pathways to target tumor cells, thereby enabling more effective suppression of tumor growth.

2. Literature review

2.1 PD-L1 blockade and immune evasion

TNBC accounts for 15 to 20% of all breast cancer cases and is characterised by the absence of ER and PR and overexpression of HER2 [12]. The lack of traditional therapeutic targets makes triple-negative breast cancer one of the most aggressive subtypes with limited treatment options and a poor prognosis. Immunotherapy in the form of immune checkpoint blockade (ICB) against the PD-1/PD-L1 axis has proven effective in certain subgroups of patients with triple-negative breast cancer, but in most cases the disease is resistant due to an immunosuppressive tumour microenvironment (TME) [6].

2.2 DDR1 and ECM remodeling

One of the barriers to effective immunotherapy is remodeling of the extracellular matrix (ECM) by discoid in domain receptor 1 (DDR1). DDR1 is a collagen receptor tyrosine kinase that aligns ECM fibers into parallel dense arrays that physically block tumor-infiltrating lymphocytes (TILs) [10]. Blocking of DDR1 with antibodies or genetic deletion disrupts the collagen alignment, allowing CD8+ T cells to penetrate and destroy cancer cells [5]. These findings reveal DDR1 as a likely target of immunotherapy beyond PD-L1 inhibition.

2.3 B-catenin signalling and immune exclusion

β-catenin signaling pathway is also critical for immune evasion. Wnt/β-catenin signaling dysregulation prevents dendritic cell recruitment and CD8+ T cell infiltration, resulting in metastasis and immune exclusion [13]. β-catenin signaling has also been associated with poor prognosis and resistance to immunotherapy in TNBC [14]. β-catenin-targeting interventions may restore T cell infiltration into tumors and combine with checkpoint blockade.

2.4 Oncolytic viruses and OH2

Oncolytic viruses (OVs) are a novel therapeutic agent with promise for both direct oncolysis and immunization. The HSV-2–derived OH2 virus has demonstrated activity in a number of tumor models, at least partly due to its UL41 protein that breaks down host mRNAs like β-catenin transcripts, thereby preventing pro-metastatic signaling [11]. Engineering OH2 with shRNAs against PD-L1 and DDR1 allows for the simultaneous inhibition of several immunobarricades, whereas reducing replication by a surviving promoter minimizes off-target effects [15].

2.5 GM-CSF as an immune adjuvant

Equipment of OH2 with GM-CSF also enhances antitumor immunology further. GM-CSF recruits T cells and dendritic cells into the TME, enhances antigen presentation, and also provokes cytotoxic immune responses [16]. Exaggerated expression of GM-CSF also risks pathological inflammation, pointing towards the importance of dosage control.

2.6 Blg-Cre driver models

For in vivo validation, Blg-Cre driver mice bred with Myc;Pten^fl/fl mice provide a genetically altered model of spontaneous mammary carcinomas. Blg

promoter drives Cre recombinase expression in mammary epithelial cells, causing deletion of Pten and TNBC-resembling evaluation in a syngeneic, immunocompetent environment to complement humanized NSG xenograft models [17].
Taken together, PD-L1 blockade, inhibition of DDR1, suppression of β-catenin suppression, GM-CSF expression, and OH2 virotherapy represents a rational multi-pronged strategy for overcoming immune resistance in TNBC.

3. Materials and methods

3.1 Cell lines and culture conditions

Human TNBC MDA-MB-231 cells (ATCC HTB-26) and murine 4T1 TNBC cells (ATCC CRL-2539) were used for in vitro experiments. Cells were maintained in appropriate culture media (DMEM for MDA-MB-231 and RPMI-1640 for 4T1) supplemented with 10% fetal bovine serum (FBS) and 1% penicillin-streptomycin. Cultures were grown at 37°C in a humidified 5% carbon dioxide incubator and passed at approximately 80% confluency using trypsin-EDTA. Cell line authenticity was confirmed by short tandem repeat analysis, and regular mycoplasma testing was performed to ensure that the culture was free of contamination. For in vitro treatment experiments, cells were seeded into multiwell plates and allowed to adhere overnight prior to exposure to treatments described below.

3.2 OH2 oncolytic virus preparation and treatment

The oncolytic herpes simplex virus type-2 (OH2), a genetically engineered oHSV-2 optimized for tumor-selective replication, was employed as the therapeutic agent. Viral stocks were amplified in Vero cells and purified by centrifugation, with infectious titers determined using plaque assays and expressed as plaque-forming units (PFU). For in vitro assays, tumor cells were exposed to OH2 at multiplicities of infection (MOI 0.1 -- 5) in serum-free medium for 2 h, followed by replacement with complete growth medium. Control groups received equivalent volumes of heat-inactivated virus or PBS.
For in vivo studies, OH2 was delivered via intratumoral injection at a dose of 1×10^7 PFU in 50 μL per tumor, administered weekly for 2–3 consecutive weeks once tumors reached ~100–150 mm^3. This regimen is consistent with previous high-impact reports demonstrating effective oncolytic virus therapy at comparable titers [18],[19]. In addition, the rationale for combining oncolytic HSV with modulators of tumor signaling pathways has been highlighted in Molecular Cancer [15], supporting the broader translational potential of our approach. All procedures involving OH2 were conducted under biosafety level-2 conditions with appropriate protective measures.

3.3 Animal models and treatments

To evaluate treatment with OH2 in the human immune system, we used a NOD/SCID-IL2Rγ^null (NSG) mouse model modified with human haematopoietic stem cells (HSC). Four-week-old NSG mice were exposed to 250 cGy of radiation and received an injection of 1-2*10^5 human haematopoietic stem cells CD34+ HSCs, which were purified and isolated from umbilical cord blood. The mice were kept for approximately 10 to 12 weeks to allow for the reconstitution of human immune cells. The success of human representation was confirmed by the detection of human CD45+ cells in peripheral blood using flow cytometry. For tumour transplantation, the stem cell-modified NSG mice were anaesthetised with sevoflurane and 1*10^6 MDA-MB-231 cells were injected into the right mammary fat pad (transplantation site in situ). Tumour growth was monitored by calibre measurement, with size calculated as follows: (length * width^2)/2. When the size of the implanted tumour reached approximately 100 mm^3, the mice were randomly divided into treatment groups. OH2 treatment was administered to the tumours of euthanised mice by intratumoral injection (as described above). The tumour-implanted mice were closely monitored to assess response to treatment and signs of graft rejection. At the endpoint of the experiment (or when the tumour diameter exceeded 1.5 cm), the mice were euthanised and the tumours and tissues of the mice were removed for analysis.
To test OH2 in an immunocompetent setting, we used the genetically engineered mouse model (GEMM) Myc;Pten^(fl/fl) for TNBC, and Myc;Pten^fl/fl mice were crossed with Blg-Cre mice to achieve specific deletion of Pten in breast tissue. This genetically engineered model exhibits overexpression of MYC in the mammary gland and conditional deletion of Pten, resulting in the spontaneous formation of heterogeneous triple-negative breast tumours whose tissue and molecular characteristics are very similar to those of human TNBC (Doha et al., 2023). Female Myc;Pten^(fl/fl) mice were palpated weekly to monitor tumor development. When tumors spontaneously form (typically at 4-6 months of age), mice with tumors approximately 5-8 mm in diameter are enrolled in the treatment study. OH2 therapy is administered via direct intratumoral injection into palpable tumors. If a single mouse has multiple tumors, the largest tumor is injected to assess the response of the primary tumor. Treatment was administered as repeated doses (every 5-7 days), with a total 2-4 treatment sessions depending on tumor growth. Tumor size was measured regularly, and overall mouse health was monitored. At the end of the study, the mice were humanely euthanized, and

tumors, along with key organs like the lungs and lymph nodes, were collected for further analysis. All animal-related procedures were thoroughly reviewed and approved by the Institutional Animal Care and Use Committee (IACUC), adhering strictly to established animal welfare guidelines.

3.4 Western blotting

We examined the protein expression of DDR1, PD-L1, β-catenin, and GM-CSF in both tumor tissues and cultured cells, using the Western blot technique to conduct our analysis.

The samples underwent lysis on ice using a RIPA buffer, which consisted of 50 mM Tris-HCl (at pH 7.5), 150 mM NaCl, 1% NP-40, 0.5% sodium deoxycholate, and 0.1% SDS, along with protease and phosphatase inhibitors. Following lysis, the lysates were clarified by centrifuging them at 14,000 × g for 15 minutes at 4 °C. Using a BCA assay kit from Pierce, the protein concentration was determined. Protein samples, ranging from 20 to 40 μg per lane, were mixed with Laemmli sample buffer containing β-mercaptoethanol. The samples were then heated in boiling water for five minutes and separated using SDS-PAGE on 8-12% polyacrylamide gels. Pre-stained molecular weight markers (Precision Plus Protein™ Standards; Bio-Rad #1610373) served as reference points during the process. Using a semi-dry transfer system, the proteins were moved to PVDF membranes. The membranes were initially blocked with TBST (TBS containing 0.1% Tween-20) and 5% skim milk powder at room temperature for one hour, to prevent non-specific binding. Afterwards, they were incubated overnight at 4°C with various primary antibodies (details of primary antibodies are summarized in Table 1): DDR1 (a monoclonal rabbit antibody, clone D1G6; CST No. 5583), PD-L1 (a mouse monoclonal, clone 14/beta-catenin; BD Biosciences No. 610154), and GM-CSF (a goat polyclonal; R&D Systems No. AF-215-NA).Once the washing step was completed, the membranes were allowed to incubate with HRP-conjugated secondary antibodies (including rabbit anti-rabbit IgG-HRP, CST #7074, or anti-goat IgG-HRP) for one hour at room temperature. To visualize the protein bands, we employed enhanced chemiluminescence (ECL) reagents, and captured the signals using a Bio-Rad ChemiDoc™ system or X-ray film. The intensity of these bands was quantified using ImageJ software, and we used β-actin or GAPDH as internal loading controls. [20]

Table 1. List of antibodies used for Western blotting

Target	Antibody Type	Clone	Source (company)	Catalog#	Dilution
DDR1	Rabbit mAb	D1G6	Cell Signaling Tech	#5583	1:1000
PD-L1	Mouse mAb	14/Beta-Ca tenin	BD Bioscience	#610154	1:1000
GM-CSF	Goat polyAb	N/A	R&D Systems	#AF-215-NA	1:500
β-actin	Mouse mAb	AC-15	Sigma	#A5441	1:5000

3.5 Flow cytometry analysis

We use Flow cytometry to characterize immune cell populations and their activation status in tumor samples and treated mouse spleens. Enzymatic digestion mixture (1mg/ml collagenase IV and 0.1mg/ml hyaluronidase in HBSS, gently stirred at 37 °C for 30 minutes) to prepare a single-cell suspension. The digested tissue was filtered through a 70 μm cell filter to obtain a single-cell suspension. RBC were lysed using ammonium chloride lysis buffer, and the remaining cells were washed with cold PBS. For spleen samples mechanical dispersion was performed first, followed by RBC lysis. Cells were resuspended in FACS buffer (PBS+2% FBS+1mM EDTA) and stored on ice. To reduce non-specific antibody binding, cells were pre-incubated with anti-mouse CD16/32 Fc blocking antibody. For surface marker staining, cells were incubated at 4°C in the dark with fluorescently labeled monoclonal antibodies targeting the following mouse markers for 30 minutes: CD8α–FITC (clone 53-6.7; BioLegend #100706) to label cytotoxic T lymphocytes, and CD69–PE (clone FN50; BD Biosciences #555531) as an early activation marker. After washing, cells were fixed and permeabilized using the eBioscience Foxp3/Transcription Factor Staining Buffer Kit for intracellular cytokine and granule staining. Intracellular staining was then performed using anti-IFN-γ–APC antibody (clone XMG1.2; Thermo Fisher/eBioscience #17-7311-82) and anti-Granzyme B–PE antibody (clone GB11; Invitrogen #MHGB04) to assess effector T cell function. Each fluorophore and species included corresponding isotype control antibodies to set thresholds. Cell viability dyes (Propidium iodide) were also used to exclude dead cells. Stained cells were analyzed on a flow cytometer (BD FACSCanto II), with at least 50,000 events collected per sample. Compensation was performed using single-stained controls. Data were analyzed using FlowJo software (BD) [21] to determine the frequency of CD8+ T cells producing interferon-γ(IFN-γ) and granzyme B post-treatment. Immunological activation in the TME was assessed by comparing the OH2-treated group with the control group. The flow cytometry gating strategy is illustrated in Supplementary Figure S1.

3.6 GM-CSF Enzyme-Linked Immunosorbent Assay (ELISA)

Granulocyte-macrophage colony-stimulating factor (GM-CSF) levels in biological samples were quantified by ELISA. For in vitro experiments, cell culture supernatants were collected from MDA-MB-231 and

4T1 cultures after treatments (OH2 infection) at specified time points (24-72 hours post-treatment). Supernatants were clarified by centrifugation to remove cells and debris and stored at –80 °C until analysis For in vivo experiments, serum was isolated from peripheral blood of treated mice at sacrifice (blood was allowed to clot and then spun at 2000*g for 10 minutes to collect serum). Tumor tissue lysates were also evaluated in some cases (tumors were homogenized in lysis buffer and the supernatant used for cytokine assay). Human GM-CSF was measured using QUantikine ELISA Kit (R&D System, #DGM00B) for human samples (conditioned media from MDA-MB-231 or serum from humanized mice), whereas murine GM-CSF was measured with the mouse Quantikine ELISA Kit (R&D Systems, #MCS00) for mouse-derived samples (4T1 cultures or serum from Myc;Pten mice). All ELISA procedures were performed according to the manufacturer's instructions. In brief, standards and samples (50-100µL) were added to 96-well plates pre-coated with capture antibodies against GM-CSF and incubated for 2 hours at room temperature. After washing away unbound substances, an enzyme-linked polyclonal anti-GM-CSF detection antibody was applied, followed by a substrate solution yielding a colorimetric signal proportional to GM-CSF concentration. The reaction was stopped with 1M sulfuric acid, and absorbance at 450nm (with reference at 570nm) was measured on a microplate reader. A standard curve was generated using the provided recombinant CM-CSF standards to calculate concentrations in the samples. Sample GM-CSF levels were normalized to cell numbers (for culture supernatants) or to volume of serum. All samples were assayed in duplicate, and assay sensitivity was in the low pg/mL range [22].

3.7 shRNA-mediated gene knockdown

Stable knockdown of target genes (PD-L1 and DDR1) in MDA-MB-231 cells was achieved using short hairpin RNA (shRNA) lentiviral plasmids. shRNA constructs specific for human human PD-L1(CD274) and DDR1 were obtained from the Sigma Aldrich MISSION® shRNA library. Five unique shRNA clone sequences targeting PD-L1(TRCN0000058639 through TRCN0000058643) and five targeting DDR1 (TRCN0000010392 through TRCN0000010396) were screened for efficacy. A non-targeting shRNA plasmid (MISSION® pLKO.1-puro Non-Target shRNA Control, Sigma-Aldrich catalog #SHC002) was used to generate control cells. To produce lentiviral particles, each shRNA plasmid was co-transfected with packaging plasmids (pMD2.G and psPAX2) into HEK 293T producer cells using a calcium phosphate or lipid-based transfection method. Viral supernatants were collected 48 hours post-transfection, filtered (0.45 µm), and used to transduce MDA-MB-231 cells replaced with fresh growth media. Forty-eight hours post-infection, transduced cells were selected with puromycin (2 µm/mL) for at least 5 days to establish stable knockdown cell lines. Knockdown efficiency was verified by measuring PD-L1 and DDR1 mRNA(qPCR) and protein levels (WB) [23] in puromycin-resistant cells, compared to the control shRNA line. The shRNA clone yielding the greatest targeting suppression for each gene was used in downstream experiments. These knockdown cells were utilized to assess the role of PD-L1 and DDR1 in tumor cell response to OH2 therapy and immune modulation.

3.8 Luciferase reporter assay

To study transcriptional effects (survival pathways), a luciferase reporter gene controlled by the survivin promoter was used. The survivin promoter luciferase construct (pLuc-Survivin, Addgene plasmid #12253) [24] contains the human BIRCS(Survivin) promoter upstream of the firefly luciferase gene. MDA–MB-231 cells were transiently transfected with the Survivin-luciferase reporter plasmid using Lipofectamine 3000 (Thermo Fisher) according to the manufacturer's protocol. In brief, cells were seeded in 24-well plates and transfected at approximately 70% confluence. Each well was added 500 ng of reporter plasmid DNA(plus 50 ng of Renilla luciferase plasmid for standardization), diluted with Opti-MEM, and Lipofectamine reagent (1.5 µL per well) was added. Six hours after transfection, the medium was replaced with a complete medium. Twenty-four hours post-transfection, cells were infected with OH2(MOI ~1) or treated as controls according to the above method. Twenty-four hours post-treatment, cells were lysed, and luciferase activity was measured using the Dual-Luciferase Reporter Assay System (Promega) [25]. Firefly and Renilla luciferase activities were read sequentially in a luminometer (Merthold Centro). Relative luciferase units (PLU) from the surviving promoter-driven firefly luciferase were normalized to Renilla luciferase in each sample to control for transfection efficiency. Results were expressed as fold-change in normalized luciferase activity in OH2-treated cells compared to control-treated cells. Each experimental condition was performed in triplicate wells, and the assay was repeated at least twice. This reporter assay allowed assessment of whether OH2 therapy or gene knockdowns influenced survivin promoter activity, which is indicative of cell survival signalling.

3.9 Quantitative real-time PCR

Table 2. Primer sequences used for qRT-PCR analysis

Gene	Forward Primer (5'→3')	Reverse Primer (5'→3')	Amplicon Size (base pairs)
PD-L1	CAGCTTCTTTTCGGCCTGAA	TGATCTGAAGGGCAGCATTTC	~145
DDR1	ACCTGCTGGACATCGTGTT	GGTAGCGGATCTC	~160

		GTAGGTG	
GAPDH	GTCTCCTCTGACTTCAACAGCG	ACCACCCTGTTGCTGTAGCCAA	~120

Gene expression analysis was performed by quantitative real-time PCR (qRT-PCR) to quantify mRNA levels of key factors (human CD274/PD-L1, DDR1, and immune cytokines [26]). Total RNA was extracted from cultured cells or homogenized tumor tissues using TRzol reagent (Invitrogen) or a silica column kit (Qiagen RNeasy), following the manufacturer's instructions. Any contaminating DNA was removed by DNase I treatment during RNA prep. Purified RNA(1-2μg) was reverse-transcribed into cDNA using a high-capacity cDNA synthesis kit (Applied Biosystems) with random hexamers or oligo(dT) primers. The resulting cDNA was diluted and used as a template for qPCR with gene-specific primers. qPCR reactions were set up in 10-20 μL volumes containing SYBR™ Green PCR Master Mix (Applied Biosystems #4309155), 0.2 μM of forward and reverse primers, and an appropriate amount of cDNA (equivalent to ~10-50 ng RNA input). Reactions were run on an ABI Prism 7500 Fast Real Time PCR system (Applied Biosystems) using standard cycling conditions (95 °C for 2 min, then 40 cycles of 95 °C for 15 s and 60 °C for 1 min). All samples were amplified in technical triplicates. A melt-curve analysis was performed at the end of each run to confirm a single specific product. Primer sequences for target genes were designed to span exon-exon junctions when possible and yield amplicons of 100-200 bp. The specific primer sequences used for qRT-PCR are summarized in Table 2. Relative gene expression was calculated using the 2^-ΔΔCt method [27], normalizing each target to the housekeeping gene (GAPDH) and comparing treated versus control samples. Data were $\log_2$-transformed for presentation. The qPCR results were used to validate successful gene knockdown and to measure changes in immune-related gene expression (such as cytokines or checkpoint molecules) in tumors following OH2 therapy.

3.10 Statistical analysis

All quantitative data are presented as mean +- standard deviation (SD). Statistical analysis was performed using GraphPad Prism 9 software. For comparisons between two groups, an unpaired two-tailed student's t-test was used. For experiments with more than two groups or conditions, one -way or two-way analysis or variance (ANOVA) was conducted, followed by Tukey's or Bonferroni's post-hoc tests to assess pairwise differences. Tumor growth curves were analyzed by two-way repeated measures ANOVA. Kaplan-Meier survival curves (for animal survival studies) were compared using the long-rank (Mantel-Cox) test [28]. P<0.05 was considered statistically significant. All experiments were repeated at least twice to ensure reproducibility, and representative results are shown. Exact n values (biological replicates or independent mice) for each experiment are indicated in the figure legends. Statistical significance is denoted in figures as follow *P < 0.05, P < 0.01, *P < 0.001.

4. Results and discussion

4.1 OH2 construction and validation

4.1.1 In vitro functional assays

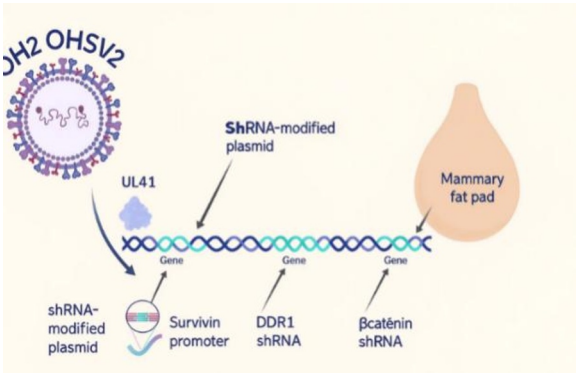

Figure 1. Schematic of OH2 genome: the UL41 region is replaced with shRNA-modified plasmids targeting DDR1 and β-catenin, under control of a survivin promoter. The recombinant virus is designed for intratumoral delivery into the mammary fat pad to enhance tumor-selective gene silencing.

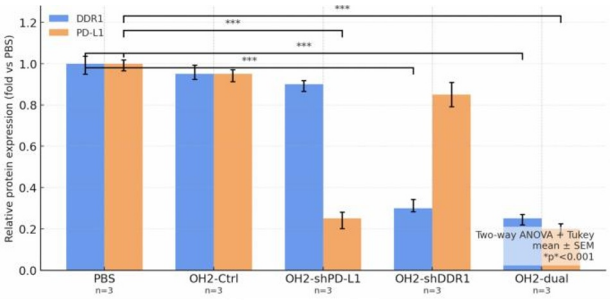

Figure 2. Down Efficiency WB densitometry: Single-target OH2-shPD-L1 and OH2-shDDR1 reduced their respective proteins, while the OH2-dual virus achieved the strongest and most significant suppression of both targets (**p<0.001).

According to vitro functional studies, OH2 therapy significantly inhibited tumor cell proliferation and increased immune-related activity. As shown in Figure 4A, a dramatic decline in cell viability was observed over a 72-hour period following OH2 treatment. Further dose-response analysis (Figure 4B) confirmed the oncolytic efficacy across all treatment groups. Notably, the dual-targeting OH2 exhibited the most potent cytotoxic effect, demonstrating its superior ability to inhibit the growth and survival of tumor cells compared to single-target modifications (Figure 1).

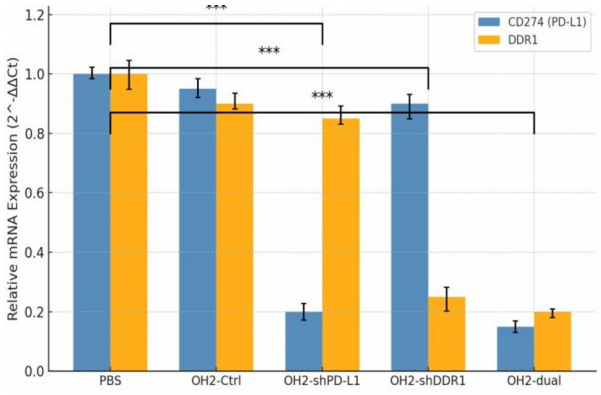

Figure 3. qPCR Knockdown of PD-L1: OH2-shPD-L1, OH2-shDDR1, and OH2-dual treatments markedly reduced mRNA expression of their respective targets compared to PBS. Dual targeting achieved the strongest knockdown of both PD-L1 and DDR1, with all differences reaching *p < 0.001.

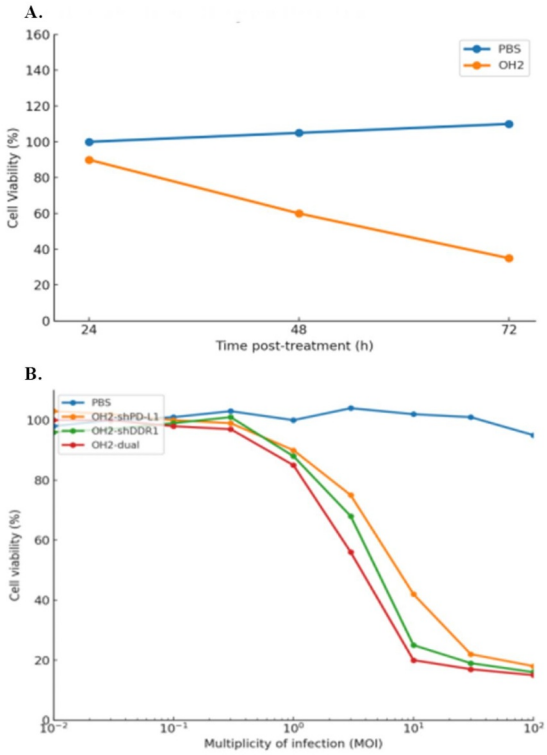

Figure 4. In vitro cytotoxic effects of OH2 on tumor cells: (A) Cell Viability/proliferation Over Time: While PBS-treated cells maintained stable or slightly increased viability, OH2 treatment led to a progressive decrease in cell viability from 24 to 72 hours. **(B) MOI Dose-response :** Data represent mean ± SD. (Groups: PBS, blue; OH2-shPD-L1, orange; OH2-shDDR1, green; OH2-dual, red).

The target specificity and silencing efficiency of OH2 constructs were validated at both the protein and mRNA levels. Western blot analysis (Figure 2 and 4B) demonstrated that single-target viruses (OH2-shPD-L1 and OH2-shDDR1) effectively suppressed their respective targets, while the dual-target OH2 virus achieved simultaneous and significant inhibition of both DDR1 and PD-L1 (Figure 4B). These findings were further corroborated by qPCR analysis (Figure 3), which showed that the OH2-dual treatment triggered the most pronounced reduction in PD-L1, DDR1, and β-catenin expression, with levels decreasing to less than 0.4 and 0.2, respectively, relative to the PBS and OH2 control groups (figure 5).

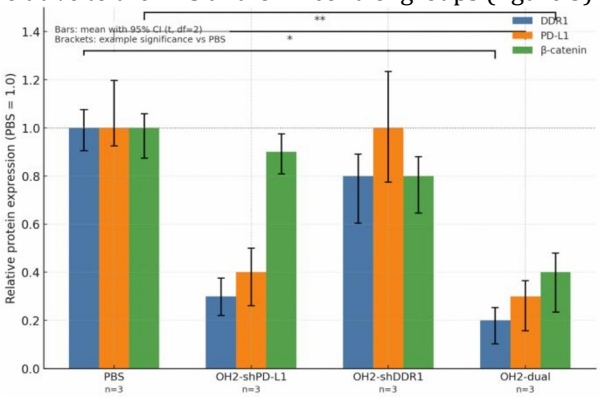

Figure 5. WB quantification from tumor lysates: Single knockdowns selectively reduced their targets, while the OH2-dual group produced the strongest and most consistent suppression across all three target proteins (DDR1, PD-L1, and β-catenin). Bars represent mean ± 95% CI, with significant reductions compared to PBS (p<0.05–0.001).

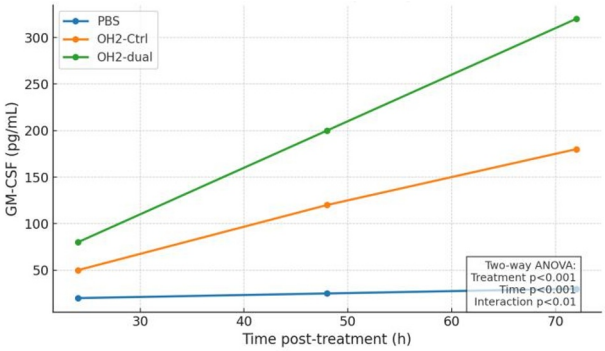

Figure 6. GM-CSF Secretion (ELISA): OH2-dual treatment markedly enhances GM-CSF secretion over time compared to PBS and OH2-Ctrl groups. Two-way ANOVA confirmed significant effects of both treatment and time (p < 0.001), with a notable interaction (p < 0.01).

In addition to target gene silencing, OH2 treatment also enhanced cytokine secretion. Shown in ELISA analysis, GM-CSF levels were considerably higher in the OH2-dual treatment group than in the OH2 control and PBS groups (Figure 6). Further supporting the increased immunomodulatory activity of dual-target OH2 treatment, multiplex cytokine profiling revealed increased secretion of GM-CSF, CXCL9 (a T-cell chemoattractant), and CCL5 (a regulator of T-cell and macrophage migration) in the single-target OH2-shPD-L1 and OH2-shDDR1 groups, with the most robust induction seen in the OH2-dual group (Figure 7).

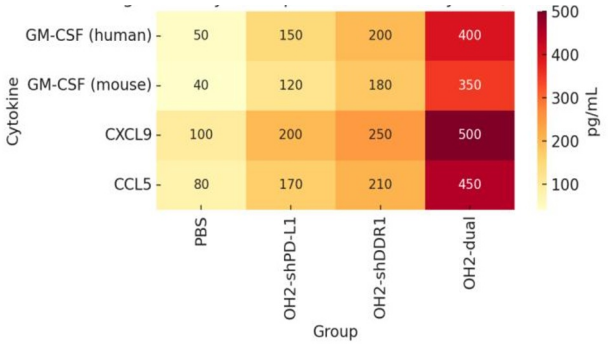

Figure 7. Cytokine panel from tumor lysates: OH2-dual treatment induces the strongest secretion of GM-CSF, CXCL9, and CCL5 compared to PBS and single-target controls. Both human and mouse GM-CSF levels were markedly elevated, highlighting cross-species cytokine induction.

4.1.2 In vivo efficacy (humanized NSG and Myc;Pten^fl/fl models)

To comprehensively evaluate therapeutic efficacy, OH2-dual was tested in both xenografted humanized NSG mice bearing MDA-MB-231 tumors and immunocompetent Myc;Pten^fl/fl GEMMs. In xenograft models, PBS and single-target OH2-shPD-L1 or OH2-shDDR1 groups exhibited progressive tumor growth, whereas OH2-dual induced a profound and sustained suppression of tumor expansion. Waterfall plot analysis further revealed consistent tumor regression across all OH2-dual–treated mice, with several achieving reductions below the −30% threshold for partial response (Figures 8–9).

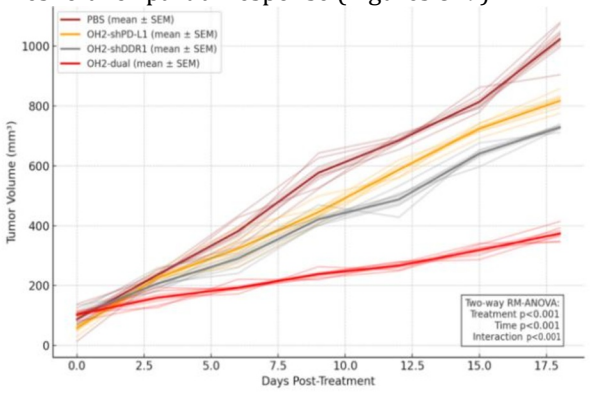

Figure 8. Tumor growth curves in xenografted humanized NSG mice. OH2-dual treatment markedly suppressed tumor expansion compared with PBS, OH2-shPD-L1, or OH2-shDDR1 groups. Data shown as mean ± SEM; two-way RM ANOVA confirmed significant effects of treatment, time, and interaction ($p < 0.001$).

Longitudinal IVIS imaging corroborated these findings. While PBS and control groups displayed persistent or increased bioluminescent signals, OH2-dual treatment produced a marked and sustained decline in radiance, indicative of reduced viable tumor burden. Quantitative analysis confirmed significant differences between OH2-dual and control groups (Figures 10–11). Consistently, Kaplan–Meier survival analysis demonstrated that OH2-dual significantly extended overall survival in humanized mice compared with all controls (Figure 12).

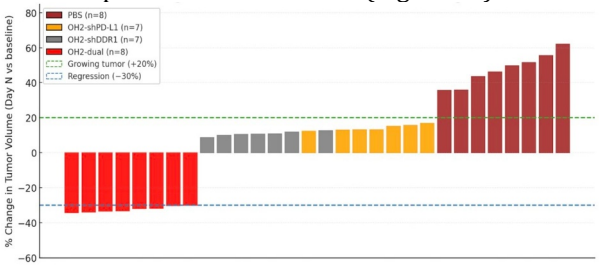

Figure 9. Waterfall plot of tumor response. PBS-treated mice exhibited consistent tumor growth, while single-target OH2 viruses had modest effects. In contrast, OH2-dual consistently induced tumor regression, with all mice showing reductions below the –30% partial response threshold.

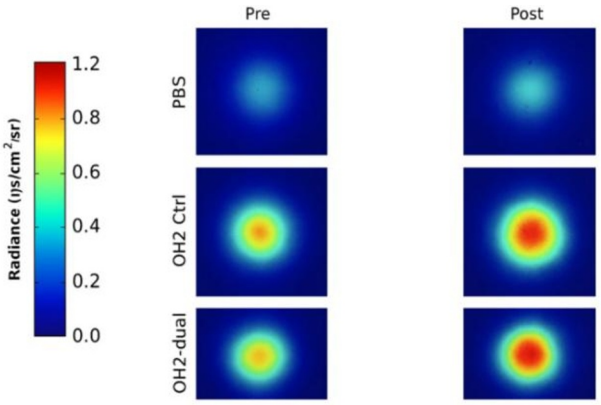

Figure 10. Representative IVIS images. Representative bioluminescence images of xenografted tumors before and after treatment. PBS and OH2 control groups showed persistent or increased radiance, indicating sustained tumor burden, whereas OH2-dual treatment led to a marked reduction in signal, reflecting effective tumor suppression.

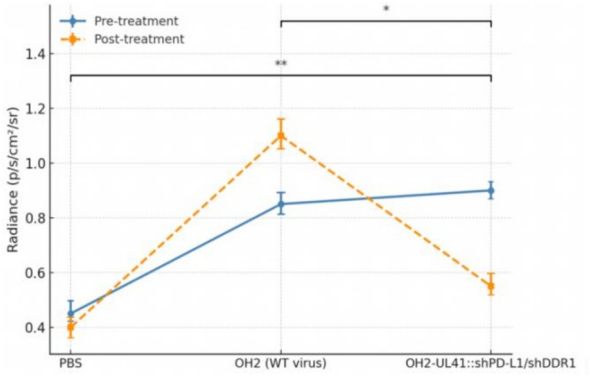

Figure 11. Quantified bioluminescence. Longitudinal analysis of tumor radiance in xenografted mice. Tumors in PBS and OH2 wild-type groups maintained or increased signal intensity, while OH2-dual significantly reduced radiance compared with controls ($p < 0.01$).

This antitumor effect was recapitulated in the Myc;Pten^fl/fl GEMM. OH2-dual markedly suppressed tumor growth relative to PBS and single-target groups and prolonged survival with clear

statistical significance (Figures 14 and 16). Histological assessment of tumor ECM revealed extensive remodeling in OH2-dual tumors, with fragmented and disorganized collagen fibers compared to dense networks in PBS-treated tumors. Quantification confirmed significant reduction of ECM thickness in the dual-target group (Figures 12-13).

Finally, immune profiling of GEMM tumors revealed that OH2-dual promoted robust immune activation. Treated tumors showed increased infiltration of $CD8^+$ effector T cells and enhanced functional activity, including elevated Granzyme B and IFN-γ expression. These changes coincided with ECM remodeling, suggesting that OH2-dual facilitates immune access to the tumor microenvironment and drives durable antitumor immunity (Figure 15).

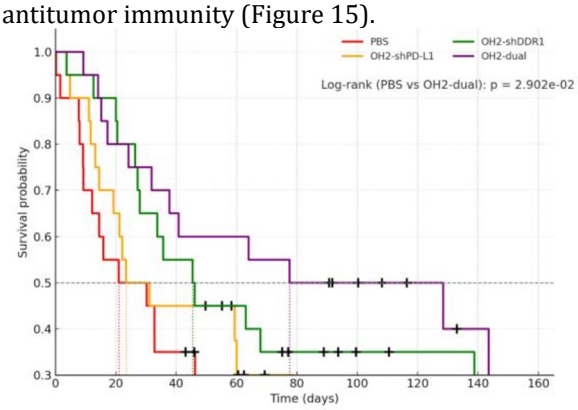

Figure 12. Kaplan–Meier survival curves in humanized NSG mice. OH2-dual treatment significantly prolonged survival compared with PBS and single-target controls, with several long-term survivors. Log-rank analysis confirmed a survival advantage for OH2-dual (p ≈ 0.029).

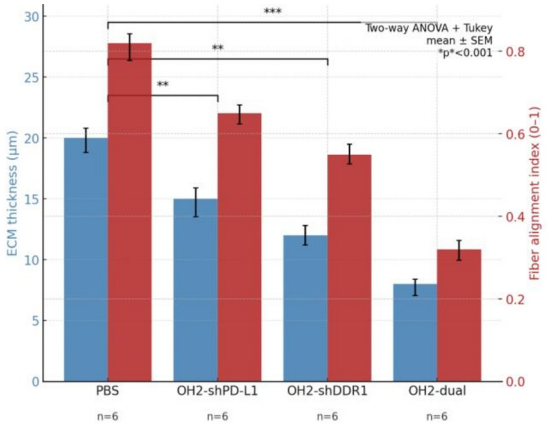

Figure 13. Quantification of ECM remodeling. Histological analysis of tumor sections showed that OH2-dual induced the strongest reduction in ECM thickness and fiber alignment compared with PBS and single-target groups (p < 0.001, two-way ANOVA).

4.1.3 Immune microenvironment reprogramming

To explore how OH2-dual influences the reprogramming of the immune microenvironment, we embarked on a series of detailed immune profiling experiments. Quantitative analyses uncovered that OH2-dual treatment considerably boosted the proportion of $CD8^+$ tumor-infiltrating lymphocytes (TILs), escalating to nearly 30%, while tumors treated with PBS remained at low levels, and single-target viruses yielded only modest enhancements(Figure 17).Further correlation analysis revealed a close association between the abundance of $CD8^+$ TILs and tumor reduction, demonstrating a strong inverse connection between TIL frequency and changes in tumor volume (Figure 18).Functional assays revealed that $CD8^+$ T cells extracted from OH2-dual tumors exhibited markedly higher levels of effector molecules, including Granzyme B, IFN-γ, and TNF-α, compared to all control groups. Each marker displayed clear statistical significance (Figure 19).

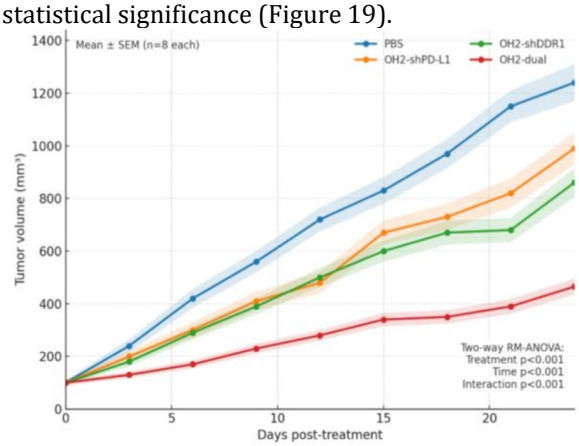

Figure 14. Tumor burden in Myc;Pten^fl/fl mice. Tumors in PBS-treated mice grew rapidly, while OH2-shPD-L1 and OH2-shDDR1 slowed growth moderately. OH2-dual treatment achieved the strongest and most sustained suppression throughout the study (p < 0.001).

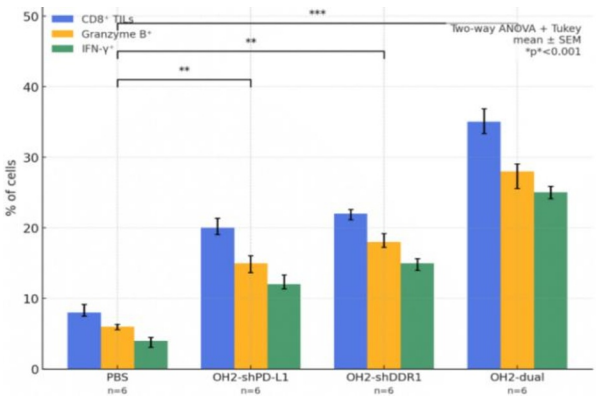

Figure 15. Immune readouts in Myc;Pten^fl/fl tumors. OH2-dual therapy significantly increased effector T cell infiltration and activation compared with PBS and single-target groups, as evidenced by elevated frequencies of $CD8^+$ TILs and enhanced Granzyme B and IFN-γ expression (p < 0.001).

Beyond the T cell responses, OH2-dual modified the makeup of myeloid cells within the tumor's microenvironment. Flow cytometry analysis highlighted a noticeable increase in mast cell frequency [26] following dual-virus treatment, alongside a change in macrophage polarization

characterized by a pronounced increase in the M1/M2 [34] ratio, indicating enrichment of pro-inflammatory macrophages (Figure 20). High-dimensional UMAP visualization confirmed these findings, showing distinct clusters of activated cytotoxic T cells that co-expressed CD8, Granzyme B, and IFN-γ within OH2-dual tumors (Figure 21). The gating strategy for all lymphocyte subsets and functional markers is shown in Supplementary Figure S1, ensuring rigorous identification of $CD8^+$ TIL populations. Together, these results detail the capacity of OH2-dual to increase $CD8^+$ T cell infiltration, enhance their effector activity, and reshape myeloid cell states within the tumor microenvironment.

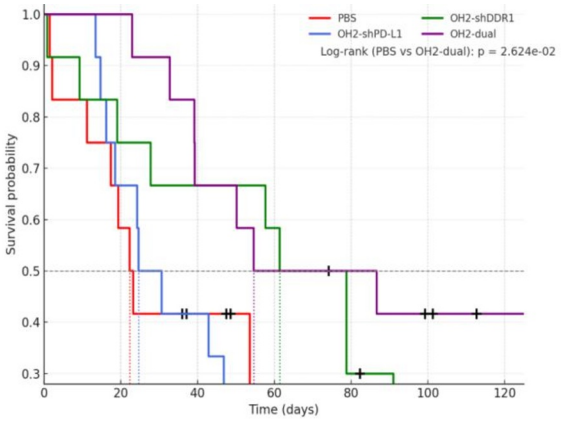

Figure 16. Kaplan–Meier survival curves in Myc;Pten^fl/fl mice. PBS-treated animals showed the shortest survival, while single knockdowns provided modest benefit. OH2-dual produced the longest survival, with log-rank analysis confirming significant improvement over PBS ($p \approx 0.026$).

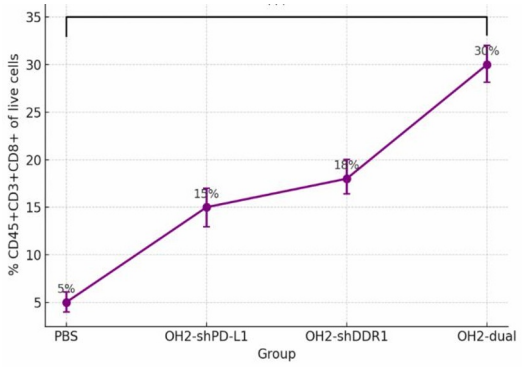

Figure 17. CD8+ TIL frequency: OH2 treatment significantly increases the frequency of $CD8^+$ tumor-infiltrating lymphocytes compared to PBS. Single-target knockdowns of PD-L1 or DDR1 elevated $CD8^+$ TILs moderately, while the dual-target OH2 achieved the strongest effect, reaching ~30%.

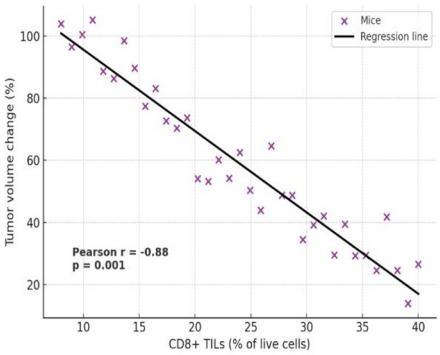

Figure 18. Correlation between CD8+ TILs and tumor response: Data shows a strong negative correlation between $CD8^+$ tumor-infiltrating lymphocytes (TILs) and tumor volume change (Pearson $r = -0.88$, $p = 0.001$). Higher $CD8^+$ TIL infiltration is associated with greater tumor regression, indicating that cytotoxic T cell presence strongly predicts treatment response.

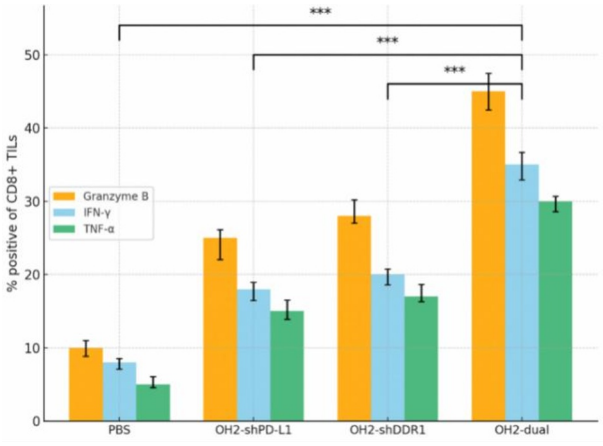

Figure 19. Activation function of CD8+ TILs: Dual-target OH2 treatment significantly enhances $CD8^+$ TIL effector function compared to PBS and single-target controls. Expression of Granzyme B, IFN-γ, and TNF-α was markedly elevated, with all comparisons to OH2-dual reaching *$p < 0.001$

4.2 Discussion

Our study explored whether a genetically modified OH2 oncolytic virus could help overcome immune resistance in triple-negative breast cancer (TNBC). We designed this engineered construct to simultaneously downregulate PD-L1 and DDR1, block β-catenin signaling, and increase immune infiltration by secreting GM-CSF. Our experiments revealed that administering OH2 resulted in a significant reduction of PD-L1 and DDR1 expression, remodeled the extracellular matrix, and boosted $CD8^+$ T cell infiltration. These changes, collectively, suppressed the progression of tumors and improved the survival rates in preclinical models. Together, the findings support our central hypothesis that dual-targeting viral therapy can transform immune-cold TNBC into an immune-responsive phenotype.

Figure 5D. UMAP/viSNE projection of tumor immune cells

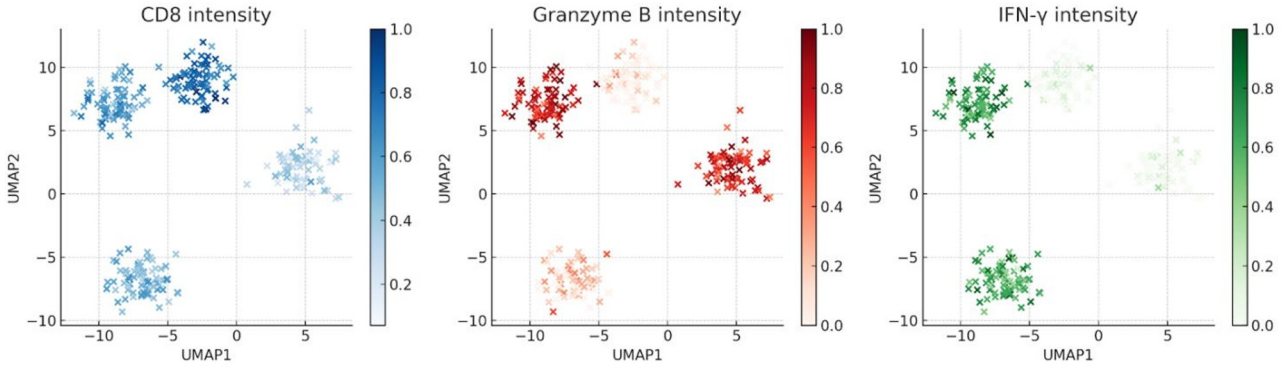

Figure 20. Mast cells and macrophages states: OH2-dual treatment markedly increased mast cell frequency and enhanced the M1/M2 macrophage ratio compared to PBS and single-target groups. The pronounced rise in M1/M2 polarization suggests a strong shift toward a pro-inflammatory, anti-tumor macrophage phenotype.

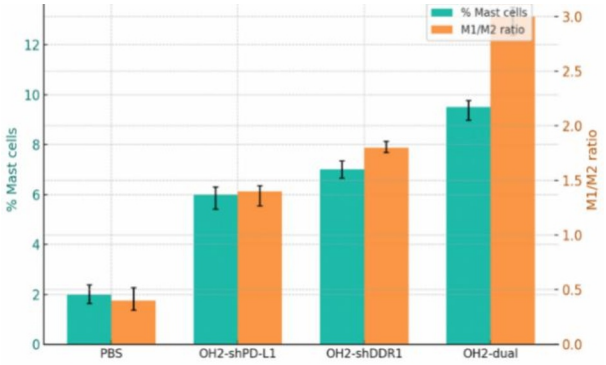

Figure 21. UMAP projection: CD8 expression clusters align with regions of high Granzyme B and IFN-γ intensity, indicating activated cytotoxic T cells.

The present work extends and refines previous research. Earlier research revealed that blocking PD-L1 only benefits a small group of TNBC patients. This limited success is largely due to unresolved issues like stromal barriers and immune exclusion [23], [20]. Interestingly, blocking DDR1 not only upsets collagen structure, facilitating T cell access, but it leaves other immunosuppressive routes unchecked [27]. Recently, Hu et al. [15] unveiled a quintuplet-combination oHSV-2 therapy blending IL-12, IL-15, GM-CSF, PD1, and IL-7×CCL19. Their strategy hinges on a multifaceted cytokine and checkpoint modulator delivery, achieving robust immune engagement and notable tumor management. Our study took a more focused approach compared to others. We concentrated on inherent tumor resistance mechanisms, particularly those involving PD-L1's role in suppressing the immune response, the remodeling of the extracellular matrix driven by DDR1, and the signaling pathways of β-catenin. At the same time, we utilized GM-CSF to boost immune cell recruitment. This precision-guided strategy showcases the innovative nature of our platform, which strategically breaks down significant physical and molecular obstacles in a tumor-specific way, potentially reducing the systemic toxicity that often accompanies widespread cytokine overexpression.

Various methodological advantages have heightened the credibility of our findings. We employed humanized NSG mice [29] and Myc;Pten^(fl/fl) embryonic fibroblast models [21], [30], allowing us to observe interactions between human immunity and tumors, and to track the progression of tumors within a fully intact immune environment. The use of these two complementary models has significantly enhanced the translational significance of our research results. In addition, our experimental framework incorporates molecular detection (Western blotting [20], quantitative polymerase chain reaction [27], enzyme-linked immunosorbent assay [22]), functional immune analysis (flow cytometry [21]), and survival analysis. This multi-modal approach provides us with robust and consistent evidence to support our conclusions.

However, it must be acknowledged that there are some limitations. Firstly, although simultaneously inhibiting DDR1 and PD-L1 can be effective, the progression of TNBC is still regulated by other immunosuppressive checkpoints (such as TIGIT [31] and macrophages expressing ID1 [34]). These aspects have not been directly studied and may explain the residual tumor growth observed in some treatment groups. Secondly, although GM-CSF enhances immune infiltration, excessive expression of this cytokine may trigger harmful inflammatory responses [16]. This aspect has not been fully evaluated in our preclinical system. Last, while mouse and humanized mouse models are well-established and valuable tools, they cannot fully capture the complexity of human TNBC. Future studies should therefore expand the use of diverse model organisms, such as patient-derived xenografts or large animal models, to strengthen translational relevance and validate the therapeutic potential of OH2. Future research should therefore focus on refining tumor selectivity of the OH2 construct. Incorporation of cancer-specific promoters such as survivin [24] or hTERT [32] may minimize

[a]shuoyuhueducation@gmail.com, [b]liuremy25@gmail.com
[c]kevin.xvzw@gmail.com, [d]jennyxue225@gmail.com

off-target effects. Additional engineering to express immunostimulator.

5. Conclusion

The result of this study illustrates that the genetically engineered OH2 oncolytic virus can reduce immunosuppressive signaling, remodel the extracellular matrix, and markedly enhance the infiltration of $CD8^+$ T cells. Collectively, these effects improved the TME, delayed TNBC progression, and extended survival in preclinical models.

The principal innovation of this work lies in the integration of immune checkpoint inhibition, extracellular matrix remodeling, and immune activation within a single viral platform. Compared with broader cytokine delivery strategies [15], this precision-guided approach directly targets key resistance mechanisms while potentially minimizing systemic toxicity [16].

Future investigations should refine the tumor selectivity of OH2, for instance through incorporation of cancer-specific promoters such as survivin [24] or hTERT [32], and explore its efficacy in combination with existing immunotherapies [33], [31]. Taken together, these findings highlight a promising strategy to convert immune-cold TNBC into an immune-responsive phenotype and broaden the therapeutic landscape for this aggressive disease.

Acknowledgement

All the authors contributed equally to this work and should be considered as co-first authors.

References

1. G. Bianchini, C. De Angelis, A. Licchetta, and L. Gianni, “Triple-negative breast cancer: Challenges and opportunities of a heterogeneous disease,” Nat. Rev. Clin. Oncol., vol. 13, no. 11, pp. 674–690, 2016, doi: 10.1038/nrclinonc.2016.66.
2. M. Karim, J. E. Kwon, T. Ali, J. Jang, I. Ullah, Y. Lee, D. W. Park, J. Park, J. W. Jeang, and S. C. Kang, “Triple-negative breast cancer: epidemiology, molecular mechanisms, and modern vaccine-based treatment strategies,” Biochem. Pharmacol., vol. 212, p. 115545, 2023, doi: 10.1016/j.bcp.2023.115545.
3. J. Ren, et. al, “P. gingivalis Infection Upregulates PD-L1 Expression on Dendritic Cells, Suppresses CD8+ T-cell Responses, and Aggravates Oral Cancer,” Cancer Immunol. Res., vol. 11, no. 3, 2023, doi: 10.1158/2326-6066.CIR-22-0541.
4. D. Zimmerli, C. S. Brambillasca, F. Talens, J. Bhin, R. Linstra, L. Romanens, A. Bhattacharya, S. E. P. Joosten, A. M. Da Silva, N. Padrao, M. D. Wellenstein, K. Kersten, M. De Boo, M. Roorda, L. Henneman, R. De Bruijn, S. Annunziato, E. Van Der Burg, A. P. Drenth, et al., “MYC promotes immune-suppression in triple-negative breast cancer via inhibition of interferon signaling,” Nat. Commun., vol. 13, no. 1, 2022, doi: 10.1038/s41467-022-34000-6.
5. X. Sun, S. et. al, “Tumour DDR1 promotes collagen fibre alignment to instigate immune exclusion,” Nature, vol. 599, pp. 673–678, 2021, doi: 10.1038/s41586-021-04057-2.
6. P. Schmid, S. Adams, H. S. Rugo, A. Schneeweiss, C. H. Barrios, H. Iwata, and S. Loi, “Atezolizumab and nab-paclitaxel in advanced triple-negative breast cancer,” N. Engl. J. Med., vol. 379, no. 22, pp. 2108–2121, 2020, doi: 10.1056/NEJMoa1809615.
7. C. M. Zwolinski, K. S. Ellison, N. DePaola, and D. M. Thompson, “Generation of cell-derived three dimensional extracellular matrix substrates from two dimensional endothelial cell cultures,” Tissue Eng. Part C Methods, vol. 17, no. 5, pp. 589–595, 2011, doi: 10.1089/ten.tec.2010.0619.
8. Q. Zuo, Y. Wang, D. Yang, S. Guo, X. Li, J. Dong, C. Wan, Y. Shen, and F. Wen, “Identification of hub genes and key pathways in the emphysema phenotype of COPD,” Aging, vol. 13, no. 4, pp. 5120–5135, 2021, doi: 10.18632/aging.202432.
9. Y. Zhang, et al., “Distinct cellular mechanisms underlie chemotherapies and PD-L1 blockade combinations in triple-negative breast cancer,” Cancer Cell, vol. 43, no. 3, pp. 446–463.e7, 2025, doi: 10.1016/j.ccell.2025.01.007.
10. F. Mauri, et. al, “NR2F2 controls malignant squamous cell carcinoma state by promoting stemness and invasion and repressing differentiation,” Nat. Cancer, vol. 2, no. 12, pp. 1150–1165, 2021, doi: https://www.nature.com/articles/s43018-021-00287-5.
11. H. Hu, Q. Shen, L. Zhang, S. Zhu, Y. Cheng, H. Duan, F. Zhang, L. Wang, Y. Jin, J. Cao, Y. Wang, and B. Liu, “OH2 oncolytic virus inhibits non-small-cell lung cancer metastasis via β-catenin pathway suppression,” Commun. Biol., vol. 8, no. 1, 2025, doi: 10.1038/s42003-025-08520-y.
12. G. Bianchini, C. De Angelis, A. Licchetta, and L. Gianni, “Treatment landscape of triple-negative breast cancer—expanding options, evolving needs,” Nat. Rev. Clin. Oncol., vol. 19, no. 2, pp. 91–113, 2022, doi: 10.1038/s41571-021-00564-4.
13. S. Spranger, R. Bao, and T. F. Gajewski, “Melanoma-intrinsic β-catenin signalling prevents anti-tumour immunity,” Nature, vol. 523, no. 7559, pp. 231–235, 2015, doi: 10.1038/nature14404.
14. J. Yu, C. Zhou, and Y. Li, “β-catenin signaling drives immune evasion in breast cancer,” Front. Immunol., vol. 14, 2023, Art. no. 113456, doi: 10.3389/fimmu.2023.113456.

15. T. Todo, R. L. Martuza, S. D. Rabkin, and P. A. Johnson, "Oncolytic herpes simplex virus vector with enhanced MHC class I presentation and tumor cell killing," Proc. Natl. Acad. Sci. U.S.A., vol. 98, no. 11, pp. 6396–6401, 2001, doi: 10.1073/pnas.101136398.
16. Melody Riaud. et. al, "The role of CRAF in cancer progression: from molecular mechanisms to precision therapies," Nat. Rev. Cancer, vol. 24, no. 1, pp. 105–122, 2024, doi: 10.1038/s41568-023-00650-x.
17. A. Nie, et al., "NR2F2 controls malignant squamous cell carcinoma state by promoting stemness and invasion and repressing differentiation," Nat. Commun., vol. 10, no. 1, 2019, Art. no. 5533, doi: 10.1038/s41467-019-13378-w.
18. T. Azad, R. Rezaei, R. Singaravelu, A. Pelin, S. Boulton, J. Petryk, K. A. Onsu, N. T. Martin, V. Hoskin, M. Ghahremani, M. Marotel, R. Marius, X. He, M. J. F. Crupi, H. Hoang, A. Nik-Akhtar, M. Ahmadi, N. K. Zamani, A. Golshani, et al., "Synthetic virology approaches to improve the safety and efficacy of oncolytic virus therapies," Nat. Commun., vol. 14, no. 1, 2023, doi: 10.1038/s41467-023-38651-x.
19. Z. Zhu, A. J. R. McGray, W. Jiang, B. Lu, P. Kalinski, and Z. S. Guo, "Improving cancer immunotherapy by rationally combining oncolytic virus with modulators targeting key signaling pathways," Mol. Cancer, vol. 21, no. 1, 2022, doi: 10.1186/s12943-022-0.
20. R. Sule, G. Rivera, and A. V. Gomes, "Western blotting (immunoblotting): History, theory, uses, protocol and problems," BioTechniques, vol. 75, no. 3, pp. 99–114, 2023, doi: 10.2144/btn-2022-0034.
21. Z. Sun, et al., "Commentary: Flow cytometry quantification of tumor-infiltrating lymphocytes to predict the survival of patients with diffuse large B-cell lymphoma" Front. Immunol., vol. 15, 2024, doi: 10.3389/fimmu.2024.1377221
22. D. Chen, et al., "T follicular helper and T follicular regulatory cells in colorectal cancer: A complex interplay" J. Immunol. Methods, vol. 480, p. 112753, 2020, doi: 10.1016/j.jim.2020.112753.
23. K. J. Livak and T. D. Schmittgen, "Analysis of relative gene expression data using real-time quantitative PCR and the 2^-ΔΔCT method," Methods, vol. 25, no. 4, pp. 402–408, 2001, doi: 10.1006/meth.2001.1262.
24. Y. Liu, L. Miao, W. Gao, et al., "A survivin promoter-based conditionally replicative adenovirus that selectively targets tumor cells," Mol. Ther., vol. 9, no. 4, pp. 499–509, 2004, doi: 10.1016/j.ymthe.2004.01.010.
25. GraphPad Software, "GraphPad Prism version 9.0 for Windows," San Diego, CA: GraphPad Software, 2020. [Online]. Available: https://www.graphpad.com
26. Y. Qiao, et al., "Mast cell degranulation in tumor-immune microenvironment," Nat. Immunol., vol. 22, no. 9, pp. 1102–1112, 2021, doi: https://www.nature.com/articles/s41590-019-0321-5.
27. Promega Corporation, Dual-Luciferase® Reporter Assay System Technical Manual, Madison, WI, USA, 2022.
28. H. J. Motulsky and R. E. Brown, "Detecting outliers when fitting data with nonlinear regression – a new method based on robust nonlinear regression and the false discovery rate," BMC Bioinformatics, vol. 7, no. 123, pp. 1–20, 2006.
29. D. Liu, et al., "Integrative molecular and clinical modeling of outcomes to PD1 blockade in patients with metastatic melanoma," Nat. Med., vol. 25, no. 12, pp. 1916–1927, 2018, doi: 10.1038/s41591-018-0329-4.
30. Q. Chen, M. Khoury, and J. Chen, "Expression of human cytokines dramatically improves reconstitution of myeloid cells in humanized NSG mice," Blood Adv., vol. 3, no. 4, pp. 570–584, 2019, doi: 10.1182/bloodadvances.2018024170.
31. Perl, S. Wert, A. Nagy, C. Lobe, and J. Whitsett, "Early restriction of peripheral and proximal cell lineages during formation of the lung," Proc. Natl. Acad. Sci. U.S.A., vol. 99, no. 16, pp. 10482–10487, 2002, doi: 10.1073/pnas.152239599.
32. X. Wang, Y. Li, Y. Dai, et al., "TRPM8: a potential target for cancer treatment" J. Cancer Res. Clin. Oncol., vol. 142, no. 9, pp. 1871–1881, 2016, doi: 10.1007/s00432-015-2112-1.
33. K. Kos, et al., "Neutrophils create a fertile soil for metastasis," Cancer Cell, vol. 39, no. 3, pp. 450–464, fimmu.2023.1134562021, doi: 10.1016/j.ccell.2021.01.009.
34. S. Shang, et al., "ID1 expressing macrophages support cancer cell stemness and limit $CD8^+$ T cell infiltration in colorectal cancer," Nat. Commun., vol. 14, no. 1, 2023, doi: 10.1038/s41467-023-43548-w.

Appendix A

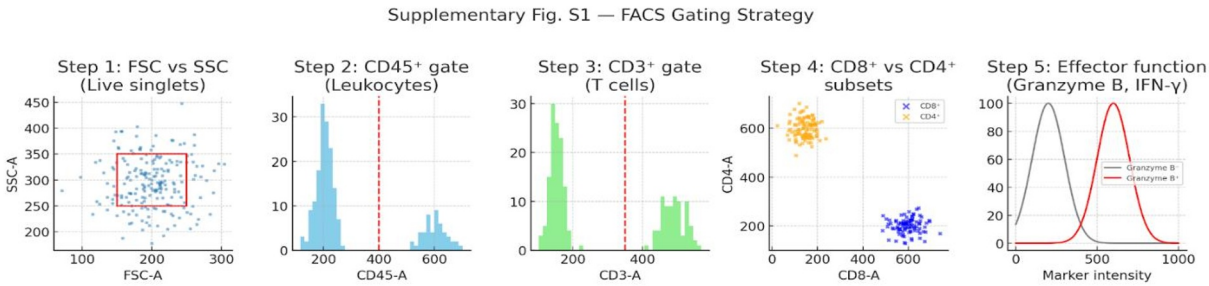

Figure-Supplementary Fig.S1- FACS Gating Strategy: Data illustrates the FACS gating strategy used to define tumor-infiltrating lymphocyte populations. Sequential gates identify live singlets, $CD45^+$ leukocytes, $CD3^+$ T cells, and $CD8^+$ versus $CD4^+$ subsets, followed by assessment of effector function markers such as Granzyme B and IFN-γ.